European Conference on Computational Fluid Dynamics
ECCOMAS CFD 2006
P. Wesseling, E. Oñate and J. Périaux (Eds)

COMPUTATIONS OF FLOWS WITH INTERFACES USING ARBITRARY LAGRANGIAN EULERIAN METHOD

Sashikumaar Ganesan[a] and Lutz Tobiska[b]

Institute of Analysis and Numerical Computation,
Otto-von-Guericke University,
PF4120, 39106 Magdeburg, Germany.
e-mail: [[a]ga.sashikumaar, [b]tobiska]@mathematik.uni-magdeburg.de
[b]web page: http://www-ian.math.uni-magdeburg.de/home/tobiska/

Key words: Two phase flows, Navier-Stokes equations, finite elements, ALE approach, Laplace-Beltrami operator

Abstract. *This work is devoted to the accurate simulation of incompressible two phase flows. The core of our methodology is the use of interface resolving meshes and the arbitrary Lagrangian-Eulerian (ALE) description of the fluid kinematics. Our numerical scheme is based on second order finite elements, a fractional step θ time discretisation, and a special approximation of the curvature to incorporate surface tension effects. We demonstrate the potential of the proposed numerical method by the simulation of a rising bubble and the Rayleigh-Taylor instability problem.*

1 INTRODUCTION

This work is concerened with the robust and efficient numerical simulation of incompressible two phase flows. In such flow problems, often, the evolution of the interface is induced by the surface force which consists of surface tension and the local curvature of the interface. Thus, an accurate representation of the interface is important in the numerical simulations to calculate the local curvature and include the surface force. Furthermore, two immiscible fluids will have different densities and viscosities, in general and therefore these physical variables will be discontinuous across the interface. It turns out that the development of robust and efficient numerical schemes for simulating fluid flows with unsteady motion of moving interfaces is still a challenging problem in computational fluid dynamics (CFD) field.

Several techniques have been proposed in the literature for simulating interface flows, see for an overview ref[1]. Based on the computation of the flow variables, velocity and pressure, all these techniques can be classified into two classes: fixed grid and moving grid methods. Each method has its own advantages and disadvantages. In fixed grid methods volume-of-fluid (VOF), level set (LS) and front-tracking (FT) are a few popular techniques used in multiphase flow simulations. In all fixed grid techniques, interfaces are not

resolved by the meshes used for the computation of the flow. This poses extra difficulty to incorporate the surface force and the material properties, when computing the flow variables. Often, the continuum surface force $(CSF)^2$ technique is used to handle the surface force in fixed grid techniques. For including the discontinuous physical variables different techniques such as defining the material property as a function of shortest distance from the interface, using a steep gradient to translate the jumps and defining the material parameters by a smoothed Heaviside function, have been proposed in the literature. However, these additional techniques in the fixed grid methods induce numerical errors in the solution, see for instance ref[3]. In the interface non-resolved meshes, spurious velocities may also be generated[4] and very fine meshes are needed (at least near the moving interface) to reduce spurious velocities. Furthermore, guarantying the mass conservation in each phase separately is also a difficult problem in fixed grid methods. Therefore, we prefer the alternative approach of moving grid technique in our computations.

In moving grid methods such as Lagrangian, arbitrary Lagrangian-Eulerian (ALE) techniques, interfaces are resolved by the meshes. Therefore, the inclusion of the surface force and the material paremeters are straight forward. In particular, we use the ALE technique in which interfaces move with the flow velocity (Lagrangian manner) and the inner points are displaced arbitrarily to reduce the distortion of meshes. Furthermore, by using appropriate pressure and curvature approximations, the spurious velocities can be avoided[4] on interface resolved the meshes.

The plan of the paper is as follows. In Section 2, we present the governing equations of two phase flow problem. Next, in Section 3, a reformulation of the model equations in the ALE framework is given. Further we describe the discretisation by finite elements and present the mesh moving technique. The numerical tests in Section 4 cover the rising bubble and the Rayleigh-Taylor instability problems. They show the capability and the accuracy of our numerical approach.

2 GOVERNING EQUATIONS

We consider an instationary two phase flow problem. Let $\Omega \subset \mathbb{R}^d$, $d \in \{2, 3\}$, be a computational domain, which consists of two immiscible liquids, say, "Liquid A" and "Liquid B". Let Ω_1 and $\Omega_2 = \Omega \setminus \Omega_1$ be the two domains of the "Liquid A" and the "Liquid B", respectively. Furthermore, let us define $\Gamma_F = \Omega_1 \cap \Omega_2$ be the interface between the two liquids "A" and "B", see Figure 1 for a 2D setting of the problem.

In the time interval $(0, \mathrm{T})$, the fluid flow in each liquid phase "A" and "B" is governed

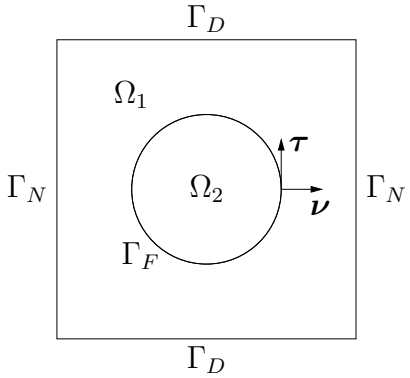

Figure 1: Two immiscible liquids are separated by the common interface Γ_F.

by the instationary Navier-Stokes equations:

$$\begin{aligned}
\rho_k \left(\frac{\partial \mathbf{u}}{\partial t} + (\mathbf{u} \cdot \nabla)\mathbf{u} \right) - \nabla \cdot (\mathbb{T}_k(\mathbf{u}, p)) &= \rho_k g \mathbf{e} && \text{in } \Omega_k(t) \times (0, \mathrm{T}), \\
\nabla \cdot \mathbf{u} &= 0 && \text{in } \Omega_k(t) \times (0, \mathrm{T}), \\
[|\mathbf{u}|] = 0, \quad \boldsymbol{\tau} \cdot [|\mathbb{T}(\mathbf{u}, p)|] \cdot \boldsymbol{\nu} &= 0 && \text{on } \Gamma_F(t) \times (0, \mathrm{T}), \\
\boldsymbol{\nu} \cdot [|\mathbb{T}(\mathbf{u}, p)|] \cdot \boldsymbol{\nu} + \sigma \mathcal{K} = 0, \quad \mathbf{u} \cdot \boldsymbol{\nu} &= \mathbf{w} \cdot \boldsymbol{\nu} && \text{on } \Gamma_F(t) \times (0, \mathrm{T}), \\
\mathbf{u} &= 0 && \text{on } \Gamma_D, \\
\mathbf{u} \cdot \boldsymbol{\nu}_N = 0, \quad \boldsymbol{\nu}_N \cdot (\mathbb{T}_1(\mathbf{u}, p)) \cdot \boldsymbol{\tau}_N &= 0 && \text{on } \Gamma_N(t) \times (0, \mathrm{T}),
\end{aligned} \tag{1}$$

for $k = 1, 2$. Here, the stress tensor $\mathbb{T}_k(\mathbf{u}, p)$ and the velocity deformation tensor $\mathbb{D}(\mathbf{u})$ are defined by

$$\mathbb{T}_k(\mathbf{u}, p) = 2\mu_k \mathbb{D}(\mathbf{u}) - p\mathbb{I}, \qquad \mathbb{D}(\mathbf{u}) = \frac{1}{2}\left(\frac{\partial u_i}{\partial x_j} + \frac{\partial u_j}{\partial x_i} \right), \quad i, j = 1, ..., d,$$

Here, $\mathbf{u}$ denotes the velocity, p the pressure, t the time, σ the surface tension coefficient, $\mathbb{I}$ the identity tensor, and $\mathcal{K}$ the sum of the principal curvature. The density and the dynamic viscosity of the liquid phases are denoted by ρ_k and μ_k, respectively. Further $\boldsymbol{\nu}_N$, $\boldsymbol{\tau}_N$ and $\boldsymbol{\nu}$, $\boldsymbol{\tau}$ denote the unit outward normal, tangential vectors of the vertical boundary Γ_N and the interface Γ_F, respectively. In the above equations, the interface velocity is denoted by $\mathbf{w}$. Furthermore, in the momentum equation, g and $\mathbf{e}$ denote the gravity and an unit vector opposite to the gravitational force. The jump across the interface Γ_F is denoted by $[|\cdot|]$ and defined for functions having traces on Γ_F by

$$[|v|] := (v|_{\Omega_1})|_{\Gamma_F} - (v|_{\Omega_2})|_{\Gamma_F}.$$

Dimensionless form

We use the material parameters of the domain Ω_1 to transform the model equations (1) into a dimensionless form. Let U_∞ and L be a characteristic velocity and a length scale.

We define the dimensionless variables as

$$\tilde{\mathbf{u}} = \frac{\mathbf{u}}{U_\infty} \quad \tilde{\mathbf{w}} = \frac{\mathbf{w}}{U_\infty} \quad \tilde{X} = \frac{X}{L}, \quad \tilde{t} = \frac{tU_\infty}{L}, \quad \tilde{p} = \frac{p}{\rho_1 U_\infty^2}.$$

Using these dimensionless variables in the stress tensor $\mathbb{T}_1(\mathbf{u}, p)$, we get

$$\begin{aligned} \mathbb{T}_1(\mathbf{u}, p) &= \rho_1 U_\infty^2 \left(\frac{2\mu_1}{\rho_1 U_\infty L} \mathbb{D}(\tilde{\mathbf{u}}) - \tilde{p}\mathbb{I} \right) = \rho_1 U_\infty^2 \left(\frac{2}{\mathcal{R}_1} \mathbb{D}(\tilde{\mathbf{u}}) - \tilde{p}\mathbb{I} \right) \\ &= \rho_1 U_\infty^2 \mathbb{S}_1(\tilde{\mathbf{u}}, \tilde{p}). \end{aligned}$$

Similarly, for the stress tensor $\mathbb{T}_2(\mathbf{u}, p)$, we get

$$\begin{aligned} \mathbb{T}_2(\mathbf{u}, p) &= \rho_1 U_\infty^2 \left(\frac{2\mu_2}{\rho_1 U_\infty L} \mathbb{D}(\tilde{\mathbf{u}}) - \tilde{p}\mathbb{I} \right) = \rho_1 U_\infty^2 \left(\frac{2}{\mathcal{R}_2} \mathbb{D}(\tilde{\mathbf{u}}) - \tilde{p}\mathbb{I} \right) \\ &= \rho_1 U_\infty^2 \mathbb{S}_2(\tilde{\mathbf{u}}, \tilde{p}). \end{aligned}$$

Here, $\mathbb{S}_k(\mathbf{u}, p)$ are the dimensionless stress tensors in the respective phases Ω_k, $k = 1, 2$. Furthermore, the dimensionless numbers

$$\mathcal{R}_1 = \frac{\rho_1 U_\infty L}{\mu_1}, \qquad \mathcal{R}_2 = \frac{\mu_1}{\mu_2} \frac{\rho_1 U_\infty L}{\mu_1} = \frac{\mu_1}{\mu_2} \mathcal{R}_1,$$

are used in the above derivations. Applying the dimensionless variable transformation to the momentum equation (the first equation in (1)) and omitting the tilde afterwards, we get

$$\rho_k \frac{U_\infty^2}{L} \left(\frac{\partial \mathbf{u}}{\partial t} + (\mathbf{u} \cdot \nabla)\mathbf{u} \right) - \rho_1 \frac{U_\infty^2}{L} \nabla \cdot (\mathbb{S}_k(\mathbf{u}, p)) = \rho_k g \mathbf{e}, \quad \text{for } k = 1, 2.$$

Note that the above equation is derived in such a way that the coefficient in front of the stress tensor term is equal in both phases. Thus, boundary conditions on the interface can be easily incorporated in the weak formulation. Furthermore, the dimensionless form the force balancing boundary condition on the interface Γ_F becomes,

$$\boldsymbol{\nu}[|\mathbb{S}(\mathbf{u}, p)|] \cdot \boldsymbol{\nu} = -\frac{\sigma}{L\rho_1 U_\infty^2} \mathcal{K}.$$

By taking $U_\infty = \sqrt{Lg}$ in the above derivations and after dividing the momentum equation by $g\ \rho_1$, we get the dimensionless form of the coupled system as

$$\begin{aligned}
\frac{\rho_k}{\rho_1}\left(\frac{\partial \mathbf{u}}{\partial t} + (\mathbf{u}\cdot\nabla)\mathbf{u}\right) - \nabla\cdot(\mathbb{S}_k(\mathbf{u},p)) &= \frac{\rho_k}{\rho_1}\mathbf{e} && \text{in } \Omega_k(t)\times(0,\mathrm{T}),\\
\nabla\cdot\mathbf{u} &= 0 && \text{in } \Omega_k(t)\times(0,\mathrm{T}),\\
[|\mathbf{u}|] = 0, \quad \boldsymbol{\tau}[|\mathbb{S}(\mathbf{u},p)|]\cdot\boldsymbol{\nu} &= 0 && \text{on } \Gamma_F(t)\times(0,\mathrm{T}),\\
\boldsymbol{\nu}[|\mathbb{S}(\mathbf{u},p)|]\cdot\boldsymbol{\nu} = -\frac{1}{Eo}\mathcal{K}, \quad \mathbf{u}\cdot\boldsymbol{\nu} &= \mathbf{w}\cdot\boldsymbol{\nu} && \text{on } \Gamma_F(t)\times(0,\mathrm{T}),\\
\mathbf{u} &= 0 && \text{on } \Gamma_D,\\
\mathbf{u}\cdot\boldsymbol{\nu}_N = 0, \quad \boldsymbol{\nu}_N\cdot(\mathbb{S}_1(\mathbf{u},p))\cdot\boldsymbol{\tau}_N &= 0 && \text{on } \Gamma_N(t)\times(0,\mathrm{T}),
\end{aligned} \tag{2}$$

for $k = 1, 2$. Here, the dimensionless Eötvös number (Eo) is defined as

$$\mathrm{Eo} = \frac{\rho_1 U_\infty^2 L}{\sigma} = \frac{\rho_1 g L^2}{\sigma}.$$

Sometimes, the Eötvös number is also called Bond number and a few authors define the Eötvös number alternatively with the density difference $(\rho_1 - \rho_2)$ between the two phases instead of the outer phase density ρ_1.

3 NUMERICAL SCHEME

The numerical scheme which we use to approximate the solution of (2) is based on an ALE approach with interface resolving meshes. We use the Laplace-Beltrami operator technique for the curvature, which avoids not only the explicit calculation of the local curvature on the interface but also allows an semi-implicit treatment of the curvature. The space and time are discretized by a second order "$inf - sup$" finite element pair and the fractional-step-ϑ scheme, respectively. We advect the interface/boundary points by the first order implicit Euler scheme, where the inner points are displaced by the elastic solid technique.

Arbitrary Lagrangian-Eulerian (ALE) Formulation

Let $\hat{\Omega}$ be a fixed reference domain and $\mathcal{A}_t$ be a family of mappings, which map each point $Y \in \hat{\Omega}$ onto the point X of the domain $\Omega(t)$ at time t. That is, for $t \in [0,\ T]$, we have

$$\mathcal{A}_t : \hat{\Omega} \to \Omega(t), \qquad \mathcal{A}_t(Y) = X(Y,t).$$

We assume that each function in the family of mappings $\mathcal{A}_t$ is homeomorphic and differentiable almost everywhere in [0, T]. By applying the chain rule with respect to time on

the relation

$$\mathbf{u}_{|_Y} = \mathbf{u}_{|_X} \circ \mathcal{A}_t,$$

we get

$$\frac{\partial \mathbf{u}}{\partial t}\Big|_Y = \frac{\partial \mathbf{u}}{\partial t}\Big|_X + \frac{\partial x}{\partial t}\Big|_Y \cdot \nabla_x \mathbf{u} = \frac{\partial \mathbf{u}}{\partial t}\Big|_X + \mathbf{w} \cdot \nabla_x \mathbf{u}. \tag{3}$$

For more details and different versions of ALE form we refer to the work of Nobile[5]. Using the relation (3) in our two phase flow model (2), the time derivative in each phase $\Omega_k(t)$ can be replaced by

$$\frac{\partial \mathbf{u}}{\partial t}\Big|_X = \frac{\partial \mathbf{u}}{\partial t}\Big|_Y - \mathbf{w}_k \cdot \nabla_x \mathbf{u} \tag{4}$$

for $k = 1, 2$. Here, $|_X$ and $|_Y$ denote the time derivative with respect to the moving domain $\Omega(t)$ and the fixed domain $\hat{\Omega}$, respectively. Furthermore, ∇_x denotes the gradient with respect to the moving domain $\Omega(t)$. In the above relation (4), the subscript k in the domain velocity $\mathbf{w}_k$ denotes that the domain velocity has to be calculated in each domain separately. Using the relation (4) in (2), we get the ALE form of the model as

$$\frac{\rho_k}{\rho_1}\left(\frac{\partial \mathbf{u}}{\partial t} + ((\mathbf{u} - \mathbf{w}_k) \cdot \nabla)\mathbf{u}\right) - \nabla \cdot (\mathbb{S}_k(\mathbf{u}, p)) = \frac{\rho_k}{\rho_1}\mathbf{e} \quad \text{in } \Omega_k(t) \times (0, \mathrm{T}), \tag{5}$$

completed by the remaining equations of (2).

Weak formulation

To simplify the notation let us introduce the notations $\Omega_{1,t} := \Omega_1(t)$, $\Omega_{2,t} := \Omega_2(t)$, and $\Omega_t := \Omega(t)$. Furthermore, we derive the weak form of (5) by defining $Q = L^2_0(\Omega_t)$ as the pressure space, and including the Dirichlet type boundary conditions in both ansatz and test spaces. The velocity space becomes

$$V := \{\mathbf{v} \in H^1(\Omega_t) : \quad \mathbf{v} \cdot \boldsymbol{\nu}_N = 0 \text{ on } \Gamma_N \quad \text{and} \quad \mathbf{v} = 0 \text{ on } \Gamma_D\}, \tag{6}$$

where $L^2(\Omega_t)$ and $H^1(\Omega_t)$ are the usual Sobolev spaces. All other boundary conditions are incorporated in the weak formulation. First, we multiply the momentum and mass equations by test functions $\mathbf{v} \in V$ and $q \in Q$, respectively. After intergrating by parts over the subdomains $\Omega_1(t)$ and $\Omega_2(t)$, separately, we incorporate the non-Dirichlet type boundary conditions on the interface Γ_F. The stress tensor term in the domain $\Omega_{1,t}$ becomes

$$\begin{aligned} -\int_{\Omega_{1,t}} \nabla \cdot \mathbb{S}_1(\mathbf{u}, p) \cdot \mathbf{v}\, dx \\ &= \int_{\Omega_{1,t}} \mathbb{S}_1(\mathbf{u}, p) : \mathbb{D}(\mathbf{v})\, dx - \int_{\Gamma_F} \mathbf{v} \cdot \mathbb{S}_1(\mathbf{u}, p)\boldsymbol{\nu}\, d\gamma \\ &= \frac{2}{\mathcal{R}_1}\int_{\Omega_{1,t}} \mathbb{D}(\mathbf{u}) : \mathbb{D}(\mathbf{v})\, dx - \int_{\Omega_{1,t}} p\nabla \cdot \mathbf{v}\, dx - \int_{\Gamma_F} \mathbf{v} \cdot \mathbb{S}_1(\mathbf{u}, p)\boldsymbol{\nu}\, d\gamma. \end{aligned} \tag{7}$$

Similarly, the stress tensor term in the domain $\Omega_{2,t}$ becomes

$$
\begin{aligned}
&-\int_{\Omega_{2,t}} \nabla \cdot \mathbb{S}_2(\mathbf{u},p)\cdot \mathbf{v}\, dx \\
&\qquad = \frac{2}{\mathcal{R}_2}\int_{\Omega_{2,t}} \mathbb{D}(\mathbf{u}) : \mathbb{D}(\mathbf{v})\, dx - \int_{\Omega_{2,t}} p\, \nabla\cdot\mathbf{v}\, dx + \int_{\Gamma_F} \mathbf{v}\cdot\mathbb{S}_2(\mathbf{u},p)\, \boldsymbol{\nu}\, d\gamma \qquad (8)
\end{aligned}
$$

Note that in the above derivations all boundary integrals except those over Γ_F vanish due to the definition of the velocity space (6) and the free slip boundary condition. After summing up the two equations (7) and (8), the interface integral term becomes

$$
\int_{\Gamma_F} \mathbf{v}\cdot[|\mathbb{S}(\mathbf{u},p)|]\boldsymbol{\nu}\, d\gamma = -\frac{1}{Eo}\int_{\Gamma_F} \mathbf{v}\cdot\mathcal{K}\boldsymbol{\nu}\, d\gamma. \qquad (9)
$$

Laplace-Beltrami operator technique

We use the Laplace-Beltrami operator technique to include the interface force (9) into the model without calculating the curvature $\mathcal{K}$, explicitly. This technique was first introduced into the finite element context by Dziuk[6]. The idea is to replace the curvature $\mathcal{K}$ by the Laplace-Beltrami operator $\underline{\Delta}$ and then apply integration by parts to the Laplace-Beltrami operator over the interface Γ_F. Hence, the interface integral (9) becomes

$$
\begin{aligned}
-\frac{1}{Eo}\int_{\Gamma_F} \mathbf{v}\cdot\mathcal{K}\boldsymbol{\nu} d\gamma_F &= -\frac{1}{Eo}\int_{\Gamma_F} \underline{\Delta} id_{\Gamma_{F,t}}\cdot\mathbf{v}\, d\gamma_F \\
&= \frac{1}{Eo}\int_{\Gamma_F} \underline{\nabla} id_{\Gamma_{F,t}} : \underline{\nabla}\mathbf{v}\, d\gamma_F,
\end{aligned}
$$

with the tangential gradient $\underline{\nabla}$, see *e.g.*, (Matthies)[7]. Here, we used the assumption that the interface Γ_F is closed. In order to use a single set of equations for the whole computational domain Ω_t and to treat the two fluid phases as one fluid with variable material properties, we define

$$
(\rho(\mathbf{x}),\ \mu(\mathbf{x})) = \begin{cases} (\rho_1,\ \mu_1) & \text{for } \mathbf{x} \text{ in } \Omega_1, \\ (\rho_2,\ \mu_2) & \text{for } \mathbf{x} \text{ in } \Omega_2, \end{cases} \quad \text{and} \quad Re(\mathbf{x}) = \begin{cases} \mathcal{R}_1 & \text{for } \mathbf{x} \text{ in } \Omega_1, \\ \mathcal{R}_2 & \text{for } \mathbf{x} \text{ in } \Omega_2. \end{cases}
$$

Hence, the weak form of the problem (5) in ALE form with Laplace Beltrami operator technique reads:

Find $(\mathbf{u},p)\in V\times Q$ such that

$$
\left(\frac{\rho}{\rho_1}\frac{\partial\mathbf{u}}{\partial t},\mathbf{v}\right) + a(\mathbf{u}-\mathbf{w},\mathbf{u},\mathbf{v}) - b(p,\mathbf{v}) + b(q,\mathbf{u}) = (f,\mathbf{v}), \quad \forall\ (\mathbf{v},q)\in V\times Q. \qquad (10)
$$

Here,

$$a(\hat{\mathbf{u}}, \mathbf{u}, \mathbf{v}) = 2\int_{\Omega_t} \frac{1}{Re}\mathbb{D}(\mathbf{u}) : \mathbb{D}(\mathbf{v})dx + \int_{\Omega_t} \frac{\rho}{\rho_1}(\hat{\mathbf{u}} \cdot \nabla)\mathbf{u} \cdot \mathbf{v}dx,$$
$$b(q, \mathbf{v}) = \int_{\Omega_t} q \ \nabla \cdot \mathbf{v}dx,$$
$$(f, \mathbf{v}) = \int_{\Omega_t} \frac{\rho}{\rho_1} \ \mathbf{e} \cdot \mathbf{v}dx - \frac{1}{Eo}\int_{\Gamma_F} \underline{\nabla} id_{\Gamma_{F,t}} : \underline{\nabla}\mathbf{v} \, d\gamma_F.$$

Here, $\mathbf{w}$ is the domain velocity in Ω_t.

Discretisation

First, we discretize the equation (10) in time using the second order Fractional-Step-ϑ scheme which is strongly A-stable, for more details see (Turek)[8]. The curvature term is discretized in time by a semi-implicit form as in ref[6]. Furthermore, the non-linear convective term is linearized by using an iteration of fixed point type. As we mentioned earlier, domains in both phases are triangulated by using interface resolving triangular meshes. The velocity is approximated by continuous, piecewise quadratics, enriched with cell bubble functions (P_2^{bubble}). The pressure is approximated by discontinuous, piecewise linear functions (P_1^{disc}). This finite element pair P_2^{bubble}/P_1^{disc} satisfies[9] the Babuška-Brezzi condition and leads to an excellent local mass conservation. Furthermore, by using the discontinuous pressure approximation on interface resolving meshes, spurious velocities can be avoided[4]. However, in order to suppress the spurious velocities genetated by the curvature approximation error and to obtain the optimal order of convergence, we have to combine the Laplace-Beltrami operator technique with isoparametric finite elements[4].

Mesh movement

First, we move the interface/boundary points (X) according to an implicit discretisation of

$$\frac{dX}{dt} = \mathbf{u}(X, t),$$

resulting to

$$X^{n+1} = X^n + (t_{n+1} - t_n)\mathbf{u}^{n+1}(X^n, t_{n+1}),$$

Then, based on the displacement of boundary points (X), the inner points are displaced in a prescribed way to preserve the mesh quality in each domain separately. Several techniques such as harmonic extension and elastic solid have been proposed in the literature to prescribe the inner points displacement, see for example, (Matthies)[7]. Among all, the elastic solid technique is generally used in case of large deformations of the domain. We move the inner mesh points in each phase Ω_{k,t_n} at each time step t_n, by solving the linear

elasticity equation for the displacement vector $\boldsymbol{\phi}$,

$$\begin{aligned} \nabla \cdot \mathbf{S}(\boldsymbol{\phi}) &= 0 && \text{in } \Omega_{k,t_n} \\ \boldsymbol{\phi} &= X^{n+1} - X^n && \text{on } \partial\Omega_{k,t_n} \end{aligned} \tag{11}$$

where

$$\mathbf{S}(\boldsymbol{\phi}) = \lambda_1(\nabla \cdot \boldsymbol{\phi})\mathbb{I} + 2\lambda_2\mathbb{D}(\boldsymbol{\phi}).$$

Here, λ_1 and λ_2 denote the Lamè constants and we use $\lambda_1 = \lambda_2 = 1$, in our computations. Continuous, piecewise linear P_1 elements on the same triangular mesh as for solving the flow equations are used for the solution of (11). Once the displacement vector $\boldsymbol{\phi}$ is known for each phase, we move all inner mesh points and calculate the domain velocity $\mathbf{w}^{n+1}$, simply by dividing $\boldsymbol{\phi}$ by the time step.

Even though the elastic update is used, it can happen that after some time the quality of the mesh becomes poor due to the large deformation in each subdomain. At that instance, we remesh the whole domain with old boundary/interface points, and interpolate the velocity and pressure from the old domain. In our calculations, we remesh the domain if the minimum angle of any mesh is less-than 10° or the maximum angle exceeds 160°. Furthermore, at some instance the interface points accumulate at one part of the interface or the resolution at some parts of the interface become inadequate. In such an instance we redistribute/add the interface points by using interpolated cubic splines.

4 NUMERICAL RESULTS

In this section, we present computational results for two different problems to show the capability and the accuracy of the proposed numerical scheme in the previous section. First, we perform computations of a rising bubble in a liquid medium. Next, we simulate the flow dynamics in the Rayleigh-Taylor instability problem. We have implemented the proposed numerical scheme in the finite element package MooNMD[10].

4.1 Rising bubble

In the rising bubble computation, we use an one-meter wide, two-meter high rectangle as the computational domain Ω_t. At time $t = 0$, the bubble is represented by a circle of radius $r_0 = 0.25$ m with center at $(0,\ 0.5)$, which is inside the rectangular domain Ω_t. As in the model (1), on the vertical boundary (Γ_N) of Ω_t we impose the free slip boundary condition, and the no-slip boundary condition on the horizontal boundaries (Γ_D) of Ω_t. Furthermore, the initial velocity is assumed to be zero, *i.e.*, $\mathbf{u}_0 = 0$ in $\Omega_{t,0}$.

The following material parameters are used in the rising bubble computation: the density $\rho_1 = 1000$ kg/m^3, $\rho_2 = 1$ kg/m^3, the dynamic viscosity $\mu_1 = 10$ kg/(m s), $\mu_2 = 0.1$ kg/(m s) and the coefficient of surface tension $\sigma = 1.96$ N/m. This set of parameters results in the dimensionless numbers $Re = 99$ and $Eo = 500$ by using a length scale $L = 1$ m.

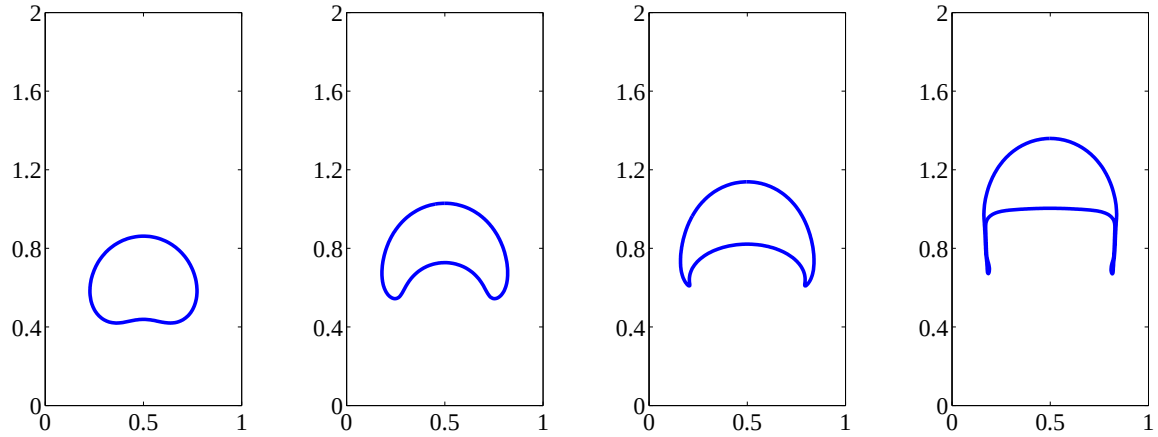

Figure 2: Shape of the rising bubble at different instance for $Re = 99$ and $Eo = 500$: time 0.75, 1.5, 2.0 and 3.0 seconds (from left to right)

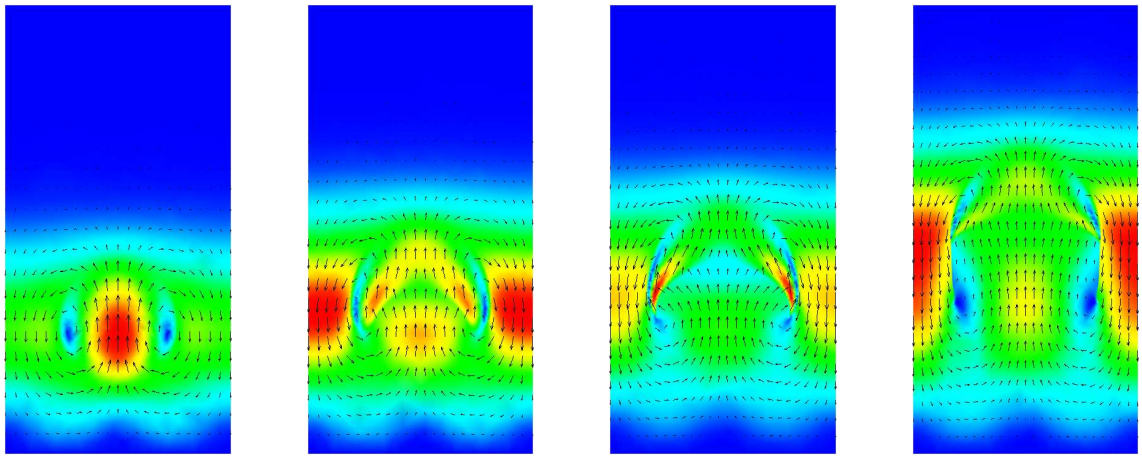

Figure 3: Flow direction in the rising bubble at different instance for $Re = 99$ and $Eo = 500$ (scale of colours represent the absolute values of the velocity): time 0.75, 1.5, 2.0 and 3.0 seconds (from left to right)

The shape of the bubble at different instances (at dimensional time $t = 0.75, 1.5, 2.0, 3.0$ seconds) for this parameter set is shown in the Figure 2. Since the Eötvös number is large ($Eo = 500$) in the considered case, the deformation of the bubble is also large. If time advances the bottom of the bubble becomes non-convex eventhough the initial shape is convex. This is due to the small surface tension coefficient and the large density ratio $\rho_1/\rho_2 = 1000$. After two seconds a tail like structure is developing on both the left and the right bottom of the bubble, which can be clearly seen in Figure 2 (fourth snapshot). Furthermore, at later stages the opposite sides of the interface along the tail become very close and additional physical knowledge has to be added to our algorithm to allow splitting

of the bubble. It should be noted that the rising bubble simulations are made in two-dimensional planar geometrical configurations. Therefore, we cannot expect quantitative agreement with the experimental results in that dimensional settings. Nevertheless, the shape of the bubble for the given Reynolds and Eötvös numbers is in good agreement with the experimental predictions (Ref. 11, Figure 2.5 on page number 27). The flow direction in the fluid and the bubble for the considered case are shown in Figure 3, where the scale of colours correspond to the absolute values of the velocity in the domain Ω_t.

4.2 Rayleigh-Taylor instability

We consider a typical test case in the area of two-phase flow problems to illustrate the capability of our numerical scheme. Using the same material parameters as in (Popinet and Zaleski)[12], we compare the shape of the interface at different instances. An one-meter wide, four-meters high rectangle is used as the computational domain Ω_t, where the upper part of the domain is occupied by a high density and the lower part by a low density liquid, respectively. We denote the upper subdomain by $\Omega_{1,t}$ and the lower by $\Omega_{2,t} = \Omega_t \setminus \Omega_{1,t}$. The material parameters are the density $\rho_1 = 1.225$ kg/m^3, $\rho_2 = 0.1694$ kg/m^3, the dynamic viscosity $\mu_1 = \mu_2 = 0.00313$ kg/(m s) and the surface tension $\sigma = 0$ N/m. These parameters result in the dimensionless number $Re = 1225.2$, by taking the length scale $L = 1$ m. Furthermore, the initial position of the interface is given by the function

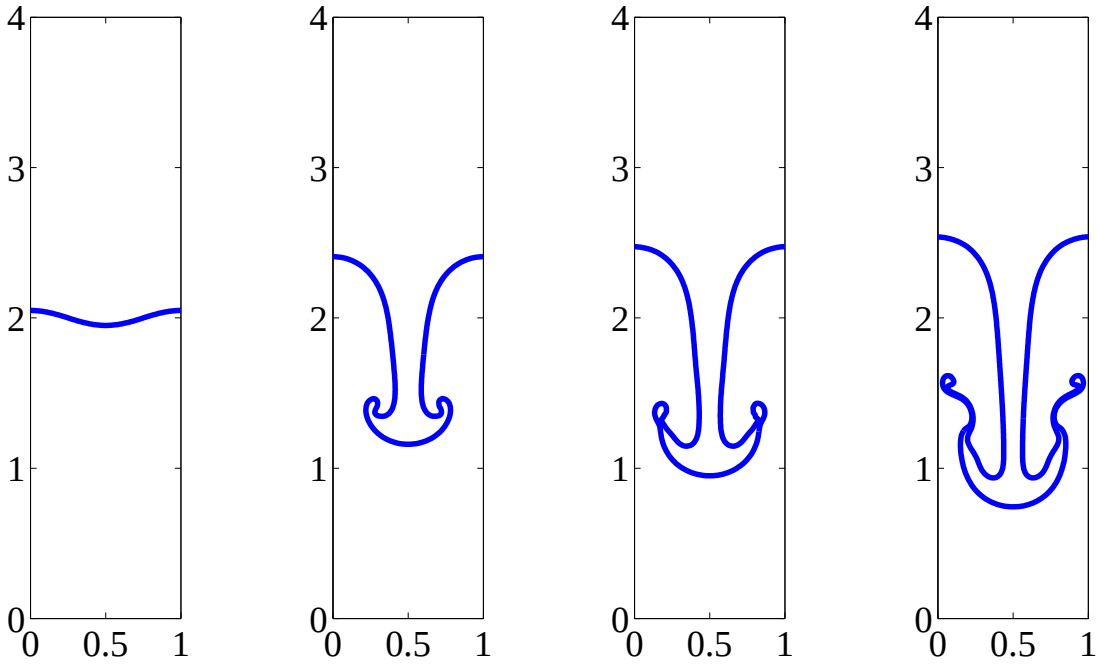

Figure 4: Shape of the interface at different instance for $Re = 1252$ with zero surface tension for the Rayleigh-Taylor instability problem: time 0, 0.7, 0.8 and 0.9 seconds (from left to right).

$y(x) = 2.0 + 0.05\cos(2\pi x)$, representing a perturbation of the flat interface. It should be noted that the interface intersects the outer boundary (Γ_N), and basically this is a moving contact line problem. Since we used the free slip boundary condition on Γ_N, the contact line singularity has been avoided. In the computation a contact angle of 90° has been used such that the general approach of handling given contact angles, see (Ganesan and Tobiska)[14], simplifies to (3). We discretize the initial domain by using approximately 2200 (increase at later stages up to 8600) triangular cells with $h_{min} = 0.01$ and $h_{max} = 0.11$. Since we use fine meshes near the interface and the interface points are evenly distributed, all the interface edges length is approximately h_{min}. The shape of the interface at different instances is shown in Figure 4 and is in very good agreement with the shape obtained in (Popinet and Zaleski)[12]. Furthermore, we calculated the mass fluctuation factor

$$M_F = \frac{\left|\Omega_{2,0} - \Omega_{2,t}\right|}{\Omega_{2,0}} \times 100\ \%.$$

In our numerical test, the mass fluctuation factor of is about $M_F = 0.009$ %, which is better than in the VOF based computation[13] (about 0.03%) with a CFL-like constrain for a similar problem. Note that there are no CFL-like constrains in our numerical scheme due to the implicit advection of the interface and the semi-implicit treatment of the curvature. In the FT based computation[12], the mass fluctuation about 0.14% has been reported for the same problem. This shows again the accuracy of the proposed numerical scheme.

Acknowledgement

This work was supported by Deutsche Forschungsgemeinschaft within in graduate program *Micro macro interactions in structured media and particle systems* (GK 828).

REFERENCES

[1] G. Tryggvason, B. Bunner, A. Esmaeeli, D. Juric, N. Al-Rawahi, W. Tauber, J. Han, S. Nas and Y.-J. Jan. A front-tracking method for the computations of multiphase flow. *J. Comput. Phys* **169**(2), 465–502, (2004).

[2] J. U. Brackbill, D. B. Kothe and C. Zemach. A continuum method for modeling surface tension. *J. Comput. Phys.* **100**, 335–354, (1992).

[3] A. K. Tornberg. *Interface tracking methods with application to multiphase flows.* PhD thesis, Royal Institute of Technology, Stockholm, (2000).

[4] F. Nobile. *Numerical approximation of fluid-structure interaction problems with application to haemodynamics.* PhD thesis, École Polytechnique Fédérale de Lausanne, (2001).

[5] G. Dziuk. An algorithm for evolutionary surfaces. *Numer. Math.* **58**, 603–611, (1991).

[6] G. Matthies. *Finite element methods for free boundary value problems with capillary surfaces.* PhD thesis, Otto-von-Guericke-Universität Magdeburg, Fakultät für Mathematik, (2002).

[7] S. Turek. *Efficient solvers for incompressible flow problems. An algorithmic and computational approach.* Springer-Verlag, Berlin, (1999).

[8] M. Crouzeix and P.-A. Raviart. Conforming and non conforming finite element methods for solving the stationary Stokes equation **I**. *R.A.I.R.O. Anal. Numér.* **7**, 33–76, (1973).

[9] S. Ganesan, G. Matthies and L. Tobiska. On spurious velocities in incompressible flow problems with interfaces. Preprint, *Fakultät für Mathematik, Otto-von-Guericke-Universität Magdeburg*, Vol. **05-35**, 1–18, (2005).

[10] V. John and G. Matthies. MooNMD - a program package based on mapped finite element methods. *Comput. Visual. Sci.* **6**, 163–170, (2004).

[11] R. Clift, J. R. Grace and M. E. Weber. *Bubbles, Drops and Particles.* Academic Press, New York, (1978).

[12] S. Popinet and S. Zaleski. A front-tracking algorithm for accurate representation of surface tension. *Int. J. Numer. Meth. Fluids.* **30**, 775–793, (1999).

[13] E. G. Puckett, A. S. Almgren, J. B. Bell, D. L. Marcus and W. J. Rider. A higher order projection method for tracking fluid interfaces in variable density incompressible flows. *J. Comput. Phys.* **100**, 269–282, (1997).

[14] S. Ganesan and L. Tobiska. Finite element simulation of a droplet impinging a horizontal surface. *In: Algoritmy 2005*, ed. by A. Handlovičová, M. Komorníková, K. Mikula, and D. Ševčovič. *Slovak Technical University, Bratislava*, 1–11, (2005).